View Online / Journal Homepage
Dynamic Article Links

Lab on a Chip

Cite this: DOI: 10.1039/c2lc40084g

www.rsc.org/loc

PAPER

Passive control of cell locomotion using micropatterns: the effect of micropattern geometry on the migratory behavior of adherent cells†

Sang-Hee Yoon,[abc] Young Kyun Kim,[ad] Eui Don Han,[e] Young-Ho Seo,[e] Byeong Hee Kim[e] and Mohammad R. K. Mofrad*[a]

Received 22nd January 2012, Accepted 7th March 2012
DOI: 10.1039/c2lc40084g

Directed cell migration is critical to a variety of biological and physiological processes. Although simple topographical patterns such as parallel grooves and three-dimensional post arrays have been studied to guide cell migration, the effect of the dimensions and shape of micropatterns, which respectively represent the amount and gradient of physical spatial cues, on cell migration has not yet been fully explored. This motivates a quantitative characterization of cell migration in response to micropatterns having different widths and divergence angles. The changes in the migratory (and even locational) behavior of adherent cells, when the cells are exposed to physical spatial cues imposed by the micropatterns, are explored here using a microfabricated biological platform, nicknamed the "Rome platform". The Rome platform, made of a biocompatible, ultraviolet (UV) curable polymer (ORMOCOMP), consists of 3 μm thick micropatterns with different widths of 3 to 75 μm and different divergence angles of 0.5 to 5.0°. The migration paths through which NIH 3T3 fibroblasts move on the micropatterns are analyzed with a persistent random walk model, thus quantifying the effect of the divergence angle of micropatterns on cell migratory characteristics such as cell migration speed, directional persistence time, and random motility coefficient. The effect of the width of micropatterns on cell migratory characteristics is also extensively investigated. Cell migration direction is manipulated by creating the gradient of physical spatial cues (that is, divergence angle of micropatterns), while cell migration speed is controlled by modulating the amount of them (namely, width of micropatterns). In short, the amount and gradient of physical spatial cues imposed by changing the width and divergence angle of micropatterns make it possible to control the rate and direction of cell migration in a passive way. These results offer a potential for reducing the healing time of open wounds with a smart wound dressing engraved with micropatterns (or microscaffolds).

1. Introduction

Cell migration is a multistep process regulated by concerted biological queues such as environmental factors, signal transduction, cytoskeletal rearrangement, *etc.* The migratory behavior of adherent cells is a sequential combination of the following processes: the morphological transformation (polarization) of a cell into a teardrop shape; the extension of the cell membrane; the formation of cell–substrate adhesions at a leading edge; the translocation of the cell body *via* contractile force; the detachment of cell–substrate adhesions at a trailing edge. Directed cell migration is essential to the development and maintenance of multicellular organisms which require the orchestrated movement of adherent cells to specified sites in particular directions.[1] Any abnormality in cell migration is known to result in serious pathophysiological consequences such as mental retardation, vascular disease, tumor formation, and metastasis.[2] A better understanding of cell migration is therefore believed to have a major impact on the development of new therapeutic strategies for the pathophysiological phenomena. For example, successful

[a]*Department of Bioengineering, University of California, Berkeley, California 94720, USA. E-mail: mofrad@berkeley.edu; Fax: +1-510-642-5835; Tel: +1-510-642-8165*
[b]*Department of Mechanical Engineering, University of California, Berkeley, California 94720, USA*
[c]*Wyss Institute for Biologically Inspired Engineering, Harvard University, Cambridge, Massachusetts 02138, USA*
[d]*Molecular Environmental Biology, University of California, Berkeley, California 94720, USA*
[e]*Medical and Bio-Material Research Center, Kangwon National University, Chuncheon 200-701, Republic of Korea*

† Electronic supplementary information (ESI) available: Optical time-sequential image of cell migration (Fig. S1), biocompatibility characterization of ORMOCOMP resin (Fig. S2–S3), analysis of cell migration controlled by micropatterns (Fig. S4 and eqn (S1)–(S2)), angular distribution of cell migration direction induced by micropatterns having different widths (Fig. S5), angular distribution of cell migration direction induced by micropatterns having different divergence angles (Fig. S6), effect of the geometry of micropatterns on cell location (Table S1), effect of the geometry of micropatterns on cell migration (Table S2), videos of cell migration along different micropatterns (Videos S1–S5). See DOI: 10.1039/c2lc40084g

control of the migratory behavior of adherent cells can lead to the effective development of new wound dressings for fast wound healing. That is, if the chemotactic migration of fibroblasts and epithelial cells is additionally expedited by new wound dressings (that passively control cell migration) during the wound healing process, the healing time of open wounds will be significantly reduced (Fig. 1a).[3,4]

Many experimental studies have been conducted to understand the migratory behavior of adherent cells since cell migration was found to be linked with many physiological

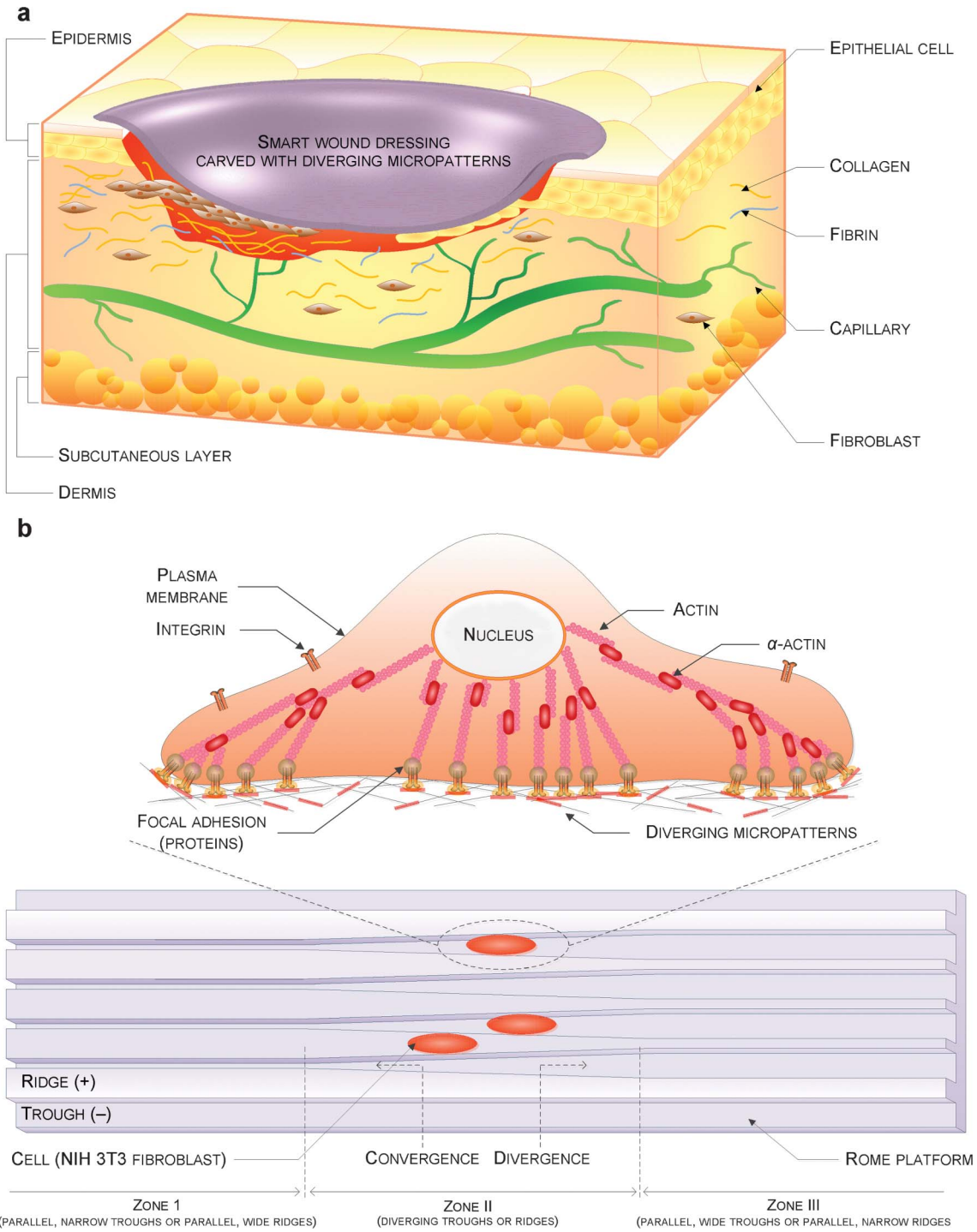

Fig. 1 A biological assay engraved with micropatterns having different widths and divergence angles, termed the Rome platform, to control cell locomotion in a passive way. (a) A conceptual drawing of smart wound dressings based on the Rome platform. The smart wound dressings, when made of biocompatible (or biodegradable) materials, direct cell migration direction and also enhance cell migration rate using the micropatterns engraved on the inner surface of the smart wound dressings. (b) A schematic of the Rome platform composed of parallel and narrow troughs (zone I), diverging troughs (zone II), and parallel and wide troughs (zone III). This assay creates the gradient of physical spatial cues using the micropatterns, thus imposing one-directional morphological polarity on adherent cells.

(*e.g.*, wound healing,[5,6] immune response,[7–9] *etc.*) and pathophysiological (*e.g.*, carcinogenesis[10–12]) processes. After R. G. Harrison found cellular response to micropatterned substrates,[13] several investigations have been conducted to characterize the effect of chemical and topographical patterns on cell–substrate interactions that regulate cell migration.[14] Chemical patterns regulated cell functions depending on their scale. In detail, *microscale* (isotropic or anisotropic) *chemical patterns* on a variety of substrates were used to locate and grow cells inside isotropic (*i.e.*, evenly spaced) islands or along anisotropic patterns.[15,16] These patterns made adherent cells align along them, which was far from controlling the migratory behavior of the cells. *Nanoscale* (isotropic or anisotropic) *chemical patterns* were studies to investigate collective cell functions (*i.e.*, adhesion, proliferation, differentiation, gene expression, *etc.*) rather than cell positioning.[17,18] Next, topographical patterns were developed to provide a biomimetic cell-stimulating cue, similar to *in vivo* textured interfaces. Cell response to topographical patterns was determined by whether the topographical patterns were isotropic or anisotropic. (Micro or nano) *isotropic topographical patterns* (*e.g.*, evenly or randomly distributed three-dimensional post arrays or porosities) were studies to examine how the isotropic topographical patterns affected collective cell behavior.[19–23] Although these studies successfully demonstrated that the scale of topography played an important role in determining whether such specific cell behavior occurred, they were unable to control the migratory behavior of adherent cells. On the other hand, (micro or nano) *anisotropic topographical patterns* (*e.g.*, parallel grooves, spikes, meshes, *etc.*) were designed to explore whether cells aligned along the anisotropic direction irrespective of micro or nanoscale.[24–31] The anisotropic topographical patterns were successful to enhance and suppress cell alignment along and across them, respectively. However, their success was still far from fully controlling cell locomotion (*e.g.*, direction and rate of cell migration).

Scientific investigations in this field have been subsequently expanded to control the migratory behavior of adherent cells. At first, cell migration was manipulated by wound healing assays that involved deliberately inflicting wounds on a confluent monolayer of adherent cells.[32–34] The wound healing assays, however, showed very limited controllability of cell migration, with virtually no control on the cell migration path. With recent advances in micromachining technology, chemotactic assays have been extensively studied to regulate the migratory behavior of adherent cells.[35–40] In these assays, the concentration distribution of chemoattractants (or chemorepellents) was adjusted using two microchambers connected to each other through a microvalve; cells and chemoattractants (or chemorepellents) were placed in each of the chambers and the gradient of chemical signals around the cells was manipulated by regulating the microvalve. Although the chemotactic assays somewhat controlled cell migration, they depended on the use of active microdevices (*i.e.*, microvalves, microregulators, *etc.*) which placed restrictions on the extent of their biomedical applications. Additionally, the chemotactic assays were unable to passively control cell migration (that is, moving an adherent cell to a specified site in a particular direction in a passive way).

Taken together with previous studies about cell response to topographical patterns, it is suggested that non-random and one-directional micropatterns control the direction and rate of cell migration and, in some cases, enhance the migratory behavior of adherent cells. We hypothesize that cell migration can be controlled by changing the width and divergence angle of micropatterns which are related to the amount and gradient of physical spatial cues (for cell migratory behavior) and the extent of controllability depends on the geometry of the micropatterns. To test this hypothesis, we developed a biological assay engraved with multiple micropatterns having different widths and divergence angles, termed the Rome platform, where all adherent cells lead to Rome (target site, Fig. 1b). The Rome platform has the following features in controlling the locomotion of adherent cells. First of all, this assay controls *cell migration direction* by imposing one-directional morphological polarity on adherent cells using micropatterns with divergence that create the gradient of physical spatial cues like *in vivo* cell migration. This assay therefore makes it possible to quantify the migratory behavior of undisturbed adherent cells in response to the micropatterns. Secondly, this assay *passively manipulates cell migration speed* by adjusting the width of micropatterns. This assay, when made of biodegradable materials (*e.g.*, poly(lactic-*co*-glycolic acid), is expected to offer a new regenerative approach for wound healing and tissue repair. Last but not least, this assay is *transparent*, which makes the assay easily incorporated with other conventional tools (*e.g.*, optical and confocal microscopes) during experimental characterization. In this paper, we passively control the locomotion of adherent cells using the Rome platform and also address the effect of the geometry of micropatterns on the locational and migratory behaviors of adherent cells. In detail, whether cell migratory characteristics such as cell migration speed, cell migration direction, directional persistence time, and random motility coefficient are determined by the amount of physical spatial cues (micropattern width) or by the gradient of physical spatial cues (divergence angle) is intensively discussed. Moreover, the upper and lower limits in the width of micropatterns which affects the migratory behavior of adherent cells are also characterized.

2. Materials and methods

2.1. Microfabrication

The first step was to make a reusable master mold on a silicon (Si) wafer. A 4 inch (500 μm thick) Si wafer was cleaned with a piranha solution of 1 : 1 (v : v) 96% sulfuric acid (H_2SO_4) and 30% hydrogen peroxide (H_2O_2) for 10 min. To prepare a master mold, 3 μm thick photoresist (SU-8 2002, MicroChem Corp.) was spin-coated at 1000 rpm for 30 s, followed by soft baking at 95 °C for 2 min, exposing at 135 mJ cm^{-2}, post exposure baking at 95 °C for 2 min, and developing with an organic solvent solution (SU-8 developer, MicroChem Corp., Fig. 2a). A polydimethylsiloxane (PDMS, MicroChem Corp.) stamp was fabricated by pouring PDMS over the SU-8 master, curing at 65 °C for 2 h, and peeling off from the SU-8 master mold (Fig. 2b). A UV-curable, hybrid polymer (ORMOCOMP US-S4, MicroChem Corp.) substrate was prepared through the spin-coating (2000 rpm, 30 s) and UV-curing (300 mJ cm^{-2} at 365 nm wavelength) of 2 ml ORMOCOMP resin on a 150 μm thick microscope cover glass that was pretreated with an oxygen plasma chamber (PM-100 Plasma Treatment System, March

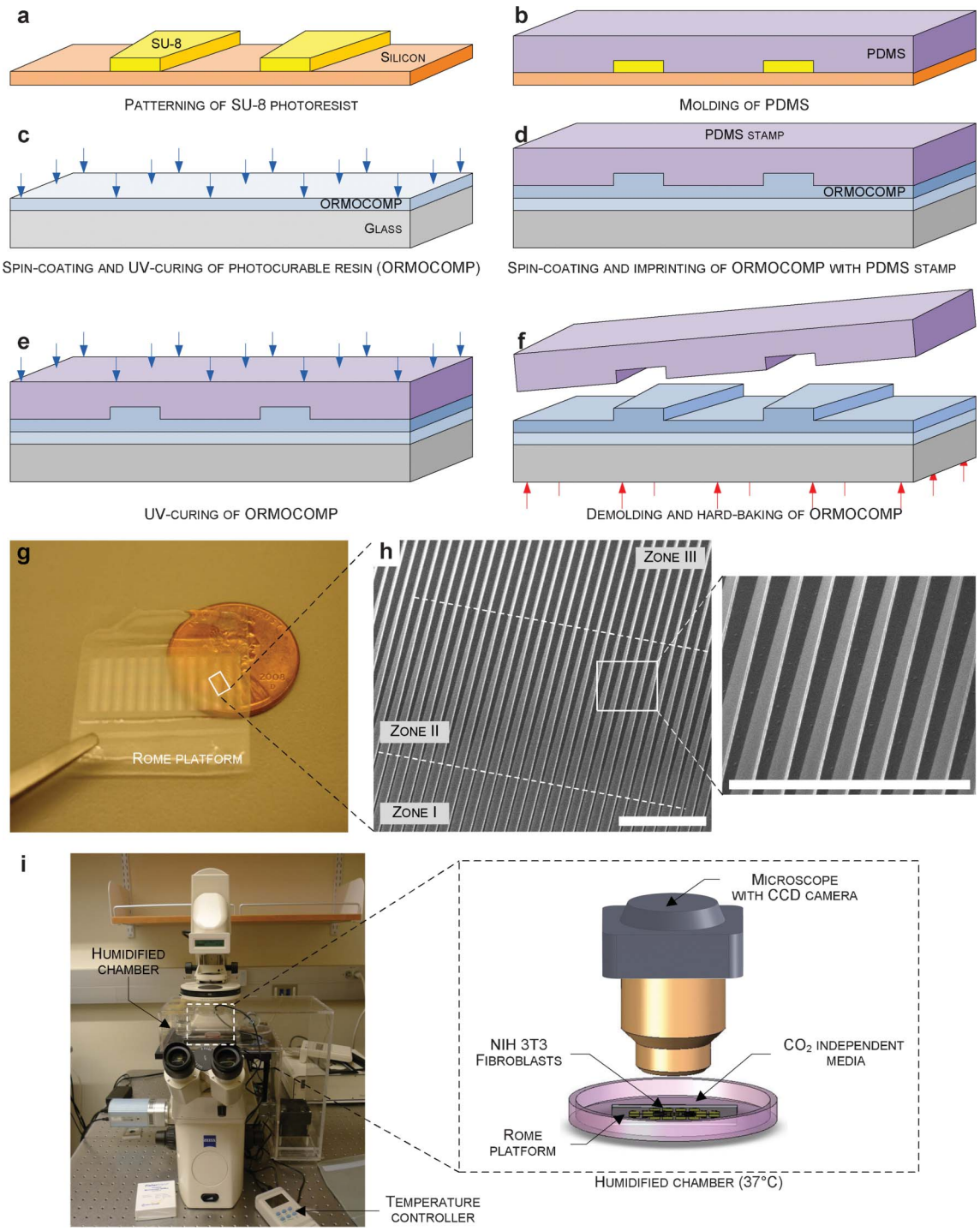

Fig. 2 Microfabrication and experimental setup of the Rome platform. (a–f) Fabrication process. (g–h) Optical (g) and scanning electron microscopy (SEM, h) images of the microfabricated assay. The optical photograph of the assay, placed on top of a one-cent coin, shows its transparency. (i) Experimental setup. Cell migration on the Rome platform is monitored with an inverted microscope equipped with a CCD camera. Scale bars of (h) are 100 μm.

Plasma Systems, Inc.) at 100 W for 30 s (Fig. 2c). After additional spin-coating of 1 ml ORMOCOMP resin and prebaking at 80 °C for 2 min, the PDMS stamp was imprinted on the ORMOCOMP layer to transfer micropatterns (Fig. 2d). This ORMOCOMP substrate was UV cured (Fig. 2e), followed by demolding and hard baking at 150 °C for 1 h (Fig. 2f).

The fabricated assay was transparent in a visual light region (Fig. 2g). Our assay consisted of parallel and narrow troughs (zone I), diverging troughs (zone II), and parallel and wide troughs (zone III), thus characterizing cell response to the micropatterns having different widths and divergence angles. The dimensions of the micropatterns were determined to be in a

compatible range with the size of NIH 3T3 fibroblasts, which were known to significantly affect the migratory behavior of the cells. Five kinds of 3 μm thick assays (Fig. 2h) had different divergence angles, θ, of 0.5 to 5.0° in zone II, a narrow width (beginning of divergence), w_b, of 3 μm in zone I, and a wide width (end of divergence), w_e, of 10 μm in zone III.

2.2. Cultivation and seeding of NIH 3T3 fibroblasts

NIH 3T3 fibroblasts with a passage number of 10 to 20, established from a NIH Swiss mouse embryo, were cultured in a Dulbecco's modified Eagle's medium (DMEM, GIBCO™) supplemented with 10% fetal bovine serum (FBS, GIBCO™) and 1% penicillin–streptomycin (Pen-Strep, GIBCO™) at 37 °C in a humidified atmosphere of 5% CO_2. Cells were passaged every four days as follows. The cells were washed once in a 1× phosphate buffered saline solution (PBS, Sigma-Aldrich) and then trypsinized with a 0.5% trypsin–EDTA solution (Sigma-Aldrich). After centrifuging the cells, they were inoculated into a new Petri dish. Before each experiment, the fabricated assay was sterilized with a 70% ethanol solution, washed twice with a 1× PBS solution, and incubated with a CO_2 independent medium (GIBCO™) supplemented with 10% FBS and 1% Pen-Strep for 1 h at room temperature. The assay was placed in a Petri dish containing a 5 ml CO_2 independent medium with a cell suspension of about 1×10^4 cells ml^{-1}. After 1 h of cell seeding, unadhered cells were removed by washing in a 1× PBS solution, followed by replacement with a fresh CO_2 independent medium supplemented with 10% FBS and 1% Pen-Strep. All experiments were conducted after 24 h of cell seeding at 37 °C in a humidified chamber.

2.3. Confocal immunofluorescence microscopy

Confocal immunofluorescence microscopy was used to assess how well NIH 3T3 fibroblasts contacted to micropatterns, that is, the contact state of the cells. Cells were fixed with a 4% (v/v) formaldehyde solution (Fisher Scientific) diluted with a chilled 1× PBS solution for 15 min. The fixed cells were permeabilized with 200 μl 0.5% (v/v) Triton X-100 (Sigma-Aldrich) diluted with a 1× PBS solution at room temperature for 10 min and washed 3 times with a 1× PBS solution, followed by blocking non-specific binding using a 3% (w/v) nonfat dry milk (Cell Signaling Technology, Inc.) diluted with a 1× PBS solution at 4 °C for 1 h and then washing the cells once with a 1× PBS solution. A 10 μl methanolic stock solution of rhodamine phalloidin (Biotium, Inc.) was diluted with a 200 μl 1× PBS solution supplemented with 1% Bovine Serum Albumin (BSA, Fisher Scientific) for each immunofluorescence staining. The actin filaments were stained by incubating the cells with this solution for 20 min at room temperature and then washing 3 times with a 1× PBS solution. Confocal immunofluorescence images were obtained with a confocal laser scanning microscope (LSM 510, Carl Zeiss MicroImaging, Inc.).

2.4. Time-lapse microscopy

Cell migration on the Rome platform was monitored with an inverted microscope (Axio Observer A1, Carl Zeiss MicroImaging, Inc.) equipped with a charge-coupled device (CCD) digital camera (Retiga-SRV, QImaging, Fig. 2i). The location of each cell was automatically tracked every half hour for 48 h using an imaging and analysis tool (QCapture PRO 5, QImaging). At least 10 cells isolated from each other were considered for statistical analysis, thus gathering 96 images from each cell, that is, total 960 images from each experiment. Experiments were repeatedly conducted at least 10 times for each assay. The migration path of each cell was tracked from the obtained time-sequential images. In detail, the coordinates of the cell (especially, nucleus), after identifying each cell, were obtained by analyzing the time-sequential images and then the relative displacement at each time interval of the cell was calculated.

2.5. Analysis of cell migration

Cell migration speed, s, was analyzed to investigate the migratory behavior of NIH 3T3 fibroblasts. Cell migration speeds at each time interval, Δt, were calculated from the relative displacement, δx and δy.

$$s = \sqrt{\left(\frac{\delta x}{\Delta t}\right)^2 + \left(\frac{\delta y}{\Delta t}\right)^2}. \quad (1)$$

Cell migration was also assessed by fitting the mean-squared displacement, $<d^2(t)>$, to a persistent random walk model, thus ultimately quantifying the directional persistence time and random migration coefficient of each cell. The mean-squared displacement was obtained from cell migration paths tracked over all experiment time. When calculating the mean-squared displacement, we used an overlapping time interval sampling method (*e.g.*, 0–1 h, 0.5–1.5 h, 1–2 h, *etc.*) over a time interval of $i\Delta t$ larger than the smallest time interval (*i.e.*, 30 min) and averaged all mean-squared displacements as follows,[41]

$$\langle d^2(t)\rangle = \frac{1}{N-i+1}\sum_{k=0}^{N-i+1}\Big[\{x((k+i)\Delta t) - x(k\Delta t)\}^2 + \{y((k+i)\Delta t) - y(k\Delta t)\}^2\Big] \quad (2)$$

where N is the total number of time intervals over the entire experiment time, x and y are the coordinates of a cell at each time interval. This equation yielded a series of $<d^2(t)>$ for increasing time interval value, $i\Delta t$. Directional persistence time and random migration coefficient were found by fitting the mean-squared displacement obtained from eqn (2) to a theoretical mean-squared displacement.[41–44]

$$<d^2(t)> = 2n_d\mu\{t - P(1 - e^{-t/P})\} \quad (3)$$

where n_d is the number of dimensions tracked in the experiments (*i.e.*, $n_d = 2$ in this analysis), μ is a random migration coefficient defined as $\mu = s^2P/n_d$,[41] and P is a directional persistence time. The values of P and μ for the cells that migrated on the Rome platform were obtained from the experimental data corresponding to one third of total cell migration because the true migration path of cells could not be monitored for enough time.[45] Some cells whose measured mean-squared displacement showed much discrepancy from the theoretical mean-squared displacement were not considered in this analysis.

Statistical analysis was conducted using a commercial statistical tool (Minitab 14, Minitab Inc.) to quantify the migratory characteristics of adherent cells (*i.e.*, cell migration speed, cell migration direction, directional persistence time, and random migration coefficient). All experimental data were analyzed by one-way analysis of variance (ANOVA) with Bonferroni *post hoc* test. *P*-values less than or equal to 0.05 were considered to indicate statistically significant. All data were represented as mean ± standard error (of the mean) values.

3. Results and discussion

To characterize the effect of the geometry of micropatterns on cell locomotion (that is, location and motion), the migratory behavior of NIH 3T3 fibroblasts migrating on the micropatterns (experimental group) was compared to that of the cells moving on a flat platform with no topographical features (control group) under the same experimental conditions. The cells were seeded on those substrates, and then the location of each cell was recorded every half hour for 48 h using time-lapse microscopy (Fig. S1a–e (ESI†) and Videos S1–S5 (ESI†)). The continuous migration paths of at least 10 cells on each substrate were tracked by analyzing the measured locations of the cells at each time interval (Fig. 3a–b). Based on the obtained time-sequential images and continuous migration paths, the locomotion of adherent cells migrating on each substrate was quantified as a function of the geometry of micropatterns, namely micropattern width and divergence angle. In this analysis, the micropattern width is used as a parameter to express the amount of physical spatial cues (that is, micropatterns), while the divergence angle is used as an index to indicate the gradient of physical spatial cues.

3.1. Biocompatibility of ORMOCOMP resin

The ORMOCOMP resin was used to fabricate the Rome platform due to the important characteristics of this resin as follows: verified biocompatibility after UV-curing;[46] cell curability without any surface modification such as fibronectin coating, collagen coating, oxygen plasma treatment, *etc.*; additional benefits of solvent-free polymerization (UV-curing) and excellent optical properties.

The different properties of substrate materials have been known to affect the adhesion nature of adherent cells which determines cell proliferation. To test the biocompatibility of the

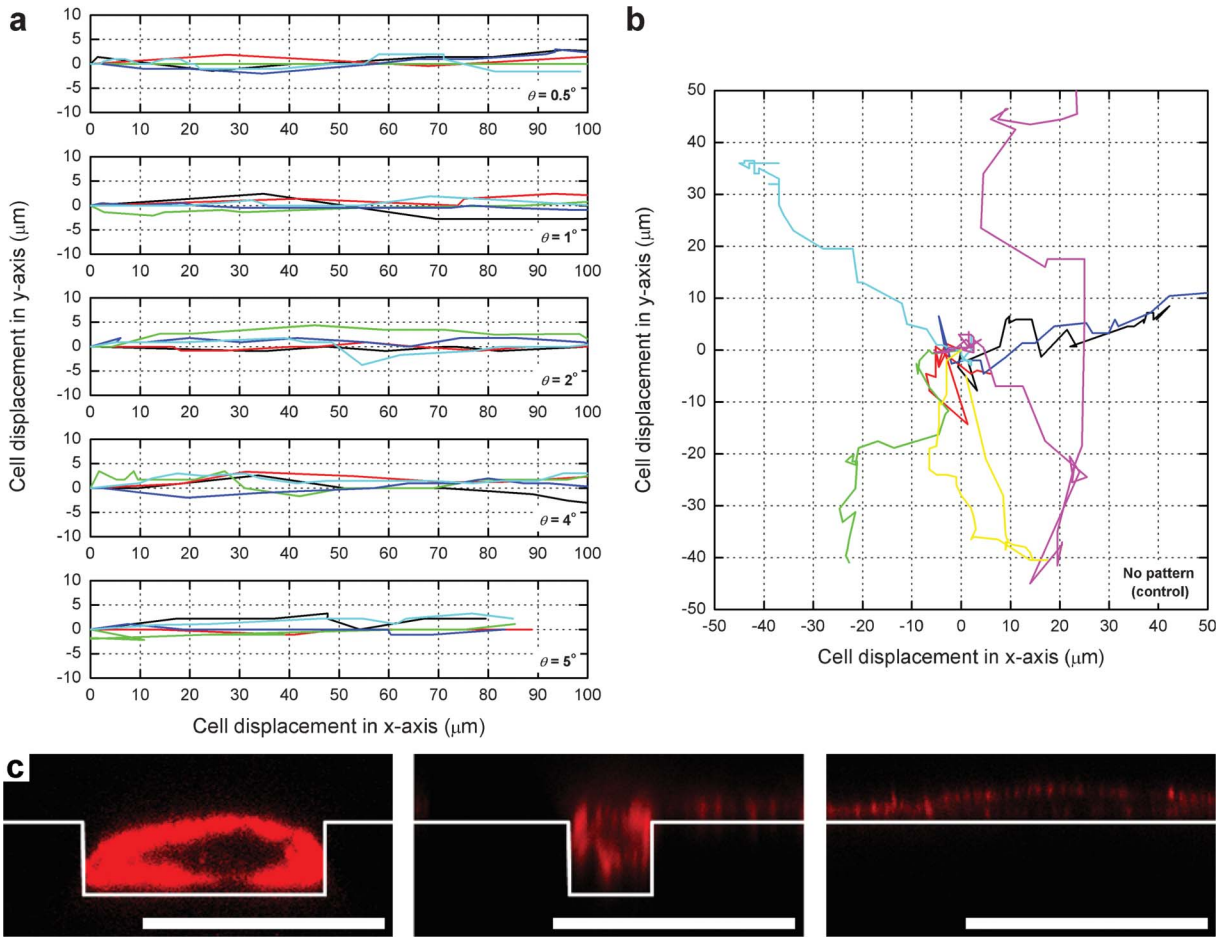

Fig. 3 Continuous migration paths of NIH 3T3 fibroblasts moving on the Rome platform. (a) Cell migration paths along the single trough of micropatterns with different divergence angles of 0.5, 1.0, 2.0, 4.0, and 5.0° (from top to bottom). (b) Cell migration paths on a flat substrate (control group 2). (c) Confocal images of the cells placed on zone III along line 1–2 of Fig. S1a (ESI†) (left), on zone I along line 3–4 of Fig. S1b (ESI†) (center), and on the flat substrate along line 5–6 of Fig. S1e (ESI†) (right). The actin filaments of the cells were stained with rhodamine phalloidin (red) for immunofluorescence imaging. Scale bars of (c) are 10 μm.

ORMOCOMP resin, NIH 3T3 fibroblasts were seeded on both a flat coverslip coated with the ORMOCOMP resin and a glass (borosilicate glass) coverslip (Ted Pella, Inc.). The glass coverslip was chosen as control group 1 because glass was known to present a favorable charge distribution on its surface and therefore to make adherent cells grow efficiently thereon.[47] The cells on both substrates were counted after different periods of cultivation, and the proliferation rate of the cells cultivated on the ORMOCOMP substrate was compared to that of the cells cultivated on the regular glass coverslip. At least 5 experiments were conducted for both substrates. The cells on the ORMOCOMP substrate proliferated at almost the same rate as those cultivated under the control conditions (Fig. S2 (ESI†)), showing that the presence of the ORMOCOMP resin did not significantly change cell growth (and cell adhesion).

In order to complete the biocompatibility tests, the morphology and viability of the cells cultivated on the ORMOCOMP substrate were compared to those of the cells cultivated on the glass coverslip using a live/dead viability kit (Invitrogen). The detailed experimental protocol used here was the same as that described in our previous study.[48] This measurement demonstrated that the investigated material secured the survival of the cells and did not alter their proliferation (Fig. S3 (ESI†)). Together with the above two experimental results, the ORMOCOMP resin can be said to be sufficiently biocompatible, unlike most other plastic materials that inhibit cell adhesion and cell growth with no extracellular matrix protein such as fibronectin, collagen, *etc.*

3.2. Micropattern effect on cell location

Next, the NIH 3T3 fibroblasts, placed on the ridges and troughs of micropatterns respectively, were counted after 24 h of cell seeding to investigate the effect of the geometry of micropatterns on cell location (not motion). When cells were cultivated on micropatterns with different widths, the cells were located on the troughs of the micropatterns more than on the ridges and the percentage of the cells placing on the troughs was inversely proportional to the width of micropatterns. This value reached 50% when the width was larger than 45.5 $\pm$ 3.5 μm (Fig. 4a and Table S1 (ESI†)). However, when the cells were cultivated on micropatterns having different divergence angles of 0.5 to 5.0° but two identical widths of 3 μm (beginning of divergence) and 10 μm (end of divergence), the percentage of the cells locating on the troughs was almost insensitive to the divergence angle (Fig. 4b and Table S1 (ESI†)). Noticeably, this percentage was in agreement with that on the micropatterns with a width of 6.5 μm (average width of the micropatterns, see Fig. 4a).

These experimental results provide us with valuable insights into the effect of the geometry of micropatterns on cell location. First, the troughs having two upward sidewalls strongly prevent cells from climbing up the micropatterns while the ridges having two downward sidewalls weakly forbid cells to fall down the micropatterns. Namely, the troughs of micropatterns are like cavities to cells that go across the micropatterns. It is easy for the cells to enter troughs (from ridges) and hard for the cells to move out of the troughs (to ridges) because the troughs hinder cell migration onto the ridges. More cells are therefore located on the troughs than on the ridges. Additionally, the degree of one-way cell movement (crossing the micropatterns) on micropatterns gets stronger as the micropattern width gets narrower, which means that the locational behavior of adherent cells is determined not by the divergence angle (gradient of physical spatial cues) but by the micropattern width (amount of physical spatial cues). These results lead to several propositions for the design of lab-on-a-chip devices that control the location of adherent cells in a passive way: a target site on which adherent cells of interest will be located should be defined by the troughs of micropatterns and not by the ridges; the troughs of micropatterns need to have a narrow width (*e.g.*, 3 μm for NIH 3T3 fibroblasts) for effective control of cell location, rather than a wide one.

3.3. Micropattern effect on cell migration direction

First of all, the dependence of cell migration direction and its angular distribution on the geometry of micropatterns were investigated. Compared to a flat substrate (control group 2) on which cells had randomly oriented protrusions and moved freely without any directionality in their migration, micropatterned substrates successfully guided the migration direction of NIH 3T3 fibroblasts using two sidewalls between two plates located on the upper and lower surfaces. On the micropatterns with no divergence (called parallel micropatterns), the guided cells travelled from left to right or *vice versa* along the micropatterns, showing their limited controllability for cell migration direction (Fig. S1a–b (ESI†)). That is, the cell migration guided by parallel micropatterns was two-directional because the micropatterns were unable to offer a one-directional gradient of physical spatial cues to the cells. In contrast, micropatterns with divergence (called diverging micropatterns) made it possible to make cells migrate in a single direction by providing the cells with a one-directional gradient of physical spatial cues (that is, divergence angle) that imposed one-directional morphological polarity on the cells (Fig. 3a, Fig. S1c (ESI†), and Fig. S4a (ESI†)).

The mechanism how diverging micropatterns made the cells move in a diverging direction of the micropatterns was understood by both cell biology and fluid mechanics. Adherent cells on the diverging micropatterns sensed the gradient of physical spatial cues and started to adopt a teardrop shape, like adherent cells *in vivo* that induced morphological polarization in response to the gradient of biochemical cues. The changes in cell morphology made the cells migrate in the diverging direction of the micropatterns.[1,49] Even when the cells initially started to travel in the opposite direction (*i.e.*, converging direction), the diverging micropatterns compelled the cells to change their migration direction (Fig. S4b–c (ESI†)). That is, the gradient of physical spatial cues imposed by the diverging micropatterns applied one-directional biochemical signals to the cells though cell–substrate interactions, thus forcing the cells to migrate in a specified direction. This one-directional cell migration on diverging micropatterns can be also analyzed with a fluid mechanics viewpoint. The cell migration guided by diverging micropatterns was assumed as a viscous flow in a rectangular microchannel (see eqn (S1)–(S2), ESI†).[50] This analysis showed that cell migration in a diverging direction had less energy loss caused by fluidic resistors than that in a converging direction. Adherent cells located on diverging micropatterns therefore

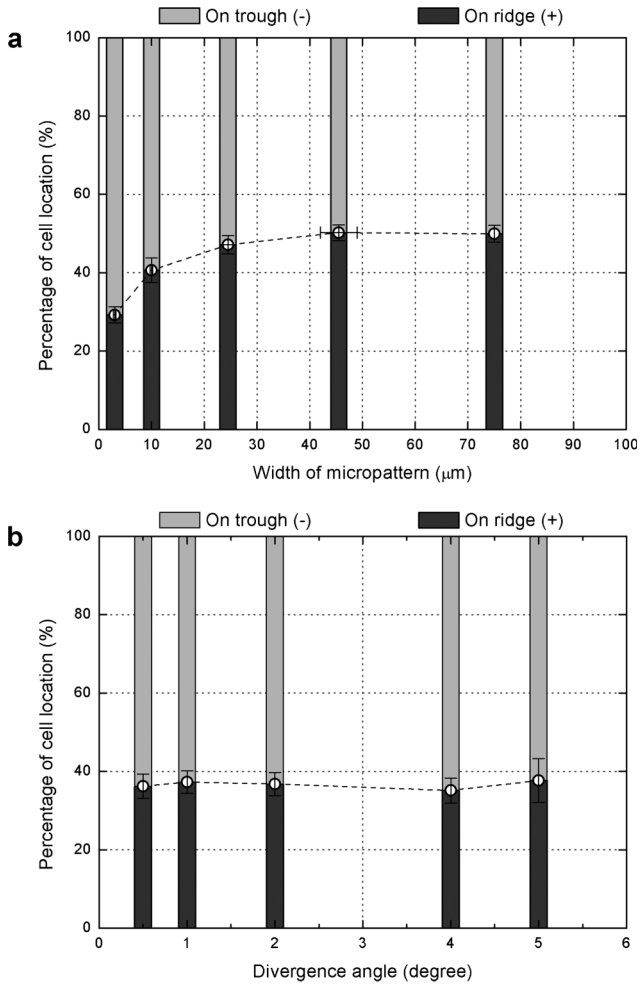

Fig. 4 Effect of the geometry of micropatterns on cell location, showing that the micropatterns have controllability for cell location. (a) Percentage of the cells locating on the troughs and ridges of micropatterns with no divergence as a function of micropattern width after 24 h of cell seeding. The data corresponding to a width of 24.5 ± 1.5 μm are obtained from the cells locating on the multiple troughs of micropatterns. (b) Percentage of the cells locating on the troughs and ridges of micropatterns with divergence as a function of divergence angle after 24 h of cell seeding. The detailed experimental data are summarized in Table S1 (ESI†).

moved in the diverging direction of the diverging micropattern, rather than in a converging direction.

Next, the effect of the geometry of micropatterns on the angular distribution of cell migration direction was characterized using continuous migration paths (Fig. 3a–b). The percentages of the cells that migrated along eight 45° angular sectors of sector 1 (0 ± 22.5°) to sector 8 (315 ± 22.5°) were respectively calculated (refer to the angle notation shown in Fig. S5a (ESI†)). NIH 3T3 fibroblasts on a flat substrate made of the ORMOCOMP resin (control group 2) moved with no directionality in their migration (Fig. 3b and Fig. S1e (ESI†)). Thus, the cells had almost the same percentage values (about 12.5%) for all angular sectors (Fig. S5a (ESI†) and Table S2 (ESI†)). When the cells were seeded on parallel micropatterns (Fig. S1a–b (ESI†)), the angular distribution of cell migration direction induced by the micropatterns was concentrated at two sectors of sectors 1 and 5 (Fig. S5b–c and Table S2 (ESI†)). In other words, most of the cells migrated along the parallel micropatterns and very few cells moved across them, showing that cell migration guided by the parallel micropatterns was two-dimensional (that is, from left to right or *vice versa* along the micropatterns). The effect of the geometry of parallel micropatterns on the degree of directionality in cell migration was explored by quantifying the percentage of the cells migrating along sector 1 of the parallel micropatterns as a function of micropattern width and relative positions (*i.e.*, troughs and ridges, Fig. 5a). The percentage of the cells migrating along sector 1 decreased as the micropattern width increased; the troughs of micropatterns were more effective than the ridges in controlling cell migration direction along the parallel micropatterns. On the diverging micropatterns with different divergence angles of 0.5 to 5.0° (Fig. 3a and Fig. S1c (ESI†)), most of the cells were guided in a diverging direction of the patterns, showing that the diverging micropatterns were able to achieve one-directional cell migration for adherent cells (Fig.

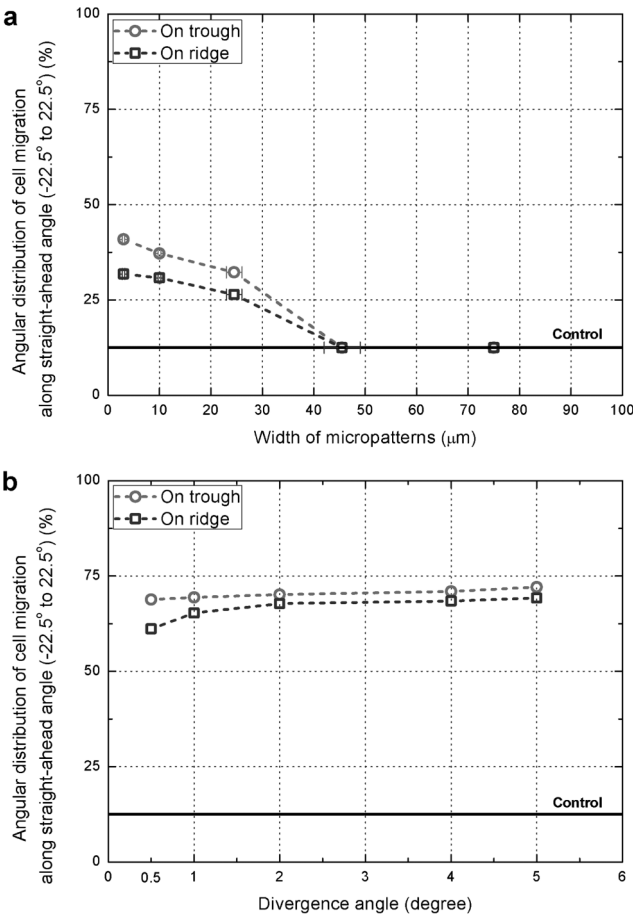

Fig. 5 Effect of the geometry of micropatterns on cell migration direction, evaluating the degree of directionality in cell migration when adherent cells are guided by each micropattern. (a) Percentage of the cells migrating along a 45° angular sector of 0 ± 22.5° as a function of micropattern width on the troughs and ridges of parallel micropatterns. (b) Percentage of the cells migrating along a 45° angular sector of 0 ± 22.5° as a function of divergence angle on the troughs and ridges of diverging micropatterns. All results are compared with that of control group 2. The detailed experimental data (including angle notation) are shown in Fig. S5–6 (ESI†) and Table S2 (ESI†).

S6 (ESI†) and Table S2 (ESI†)). The larger the divergence angle of the micropatterns, the more cells the diverging micropatterns compelled to move along a sector; even on the diverging micropatterns, the troughs made the cells migrate in the specified direction (*i.e.*, diverging direction of the diverging micropatterns) more than the ridges (Fig. 5b).

The experimental results show the following biological facts. The physical spatial cues imposed by micropatterns are enough to force adherent cells to move along the micropatterns rather than across them; adherent cells, when sensing the physical spatial cues, stretch themselves along the cues to maximize their contact area (see Fig. 3c); this morphological change in the cells results in the contact guidance of cell migration along the micropatterns. Secondly, the degree of change in cell morphology defined by the geometry of micropatterns (*e.g.*, width for parallel micropatterns, divergence angle for diverging micropatterns) determines the level of the tendency to guide cell migration direction; this confirms that the morphological change in cells is correlated to the direction of cell migration. Thirdly, a controlled gradient of physical spatial cues (like the divergence angle of micropatterns) is a sufficient condition to decide cell migration direction because adherent cells sense the gradient and then migrate in the specified direction. Last but not least, the troughs of micropatterns enforce this tendency (that is, guiding cell migration direction) by hindering cell movement onto the ridges, which makes the cells keep their migration track on the troughs more than on the ridges.

3.4. Micropattern effect on cell migration speed (migratory characteristics)

We also characterized the effect of the geometry of micropatterns on cell migratory characteristics such as cell migration speed, directional persistence time, and random motility coefficient. The cell migration speed means the rate at which adherent cells move on micropatterns; the directional persistence time indicates how long the cells maintain their migration without significant changes in cell migration direction; the random motility coefficient represents how much the cells disperse on the micropatterns. These cell migratory characteristics were determined by analyzing the measured cell migration paths (Fig. 3a–b) with a persistent random walk model.[41–44] The cell migratory characteristics were separated and quantified in terms of micropattern widths (w_b and w_e) and divergence angle (θ) where w_b and w_e are two widths of micropatterns at which the divergence of the micropatterns with a divergence angle of θ begins and ends, respectively (see Fig. S4a (ESI†)). All measurements are summarized in Table S2 (ESI†).

3.4.1. Dependence of cell migratory characteristics on micropattern width. The effect of micropattern width on cell migration speed was explored using the Rome platform. The cell migration speed (s), calculated from eqn (1), showed an inverse relation to the micropattern width (w_c), represented as s (μm min^{-1}) = 0.26 + 0.88/w_c (μm) where $w_c = (w_b + w_e)/2$ for diverging micropatterns (Fig. 6a). The cell migration speed measured on the micropatterns with a width of 45.5 ± 3.5 μm was identical to that obtained from a flat substrate (control group 2), indicating the micropatterns with a width of larger than 45.5 ± 3.5 μm were recognized as a flat substrate by the cells. Remarkably, when the cell contacted to multiple (more than one), parallel micropatterns (denoted with an asterisk symbol in Fig. 6a–c), its migration speed was determined by the largest width to which the circumferential marginal zone of the cell was contacting (see Fig. S1d (ESI†)). Next, the dependence of directional persistence time on micropattern width was explored. The directional persistence time got maximized at a micropattern width of 10 μm (Fig. 6b). In other words, the cells migrating on the micropatterns with a too narrow width ($w_c < 10$ μm) easily changed their migration direction because they had a relatively small contact area to the micropatterns and sensed other physical spatial cues around the micropatterns, whereas other cells travelling on the micropatterns with a too wide width (10 μm $< w_c <$ 45.5 ± 3.5 μm) incompletely sensed the micropatterns, thus frequently changed their migration direction. The random motility coefficient was also calculated as a function of micropattern width (Fig. 6c). The random motility coefficient was inversely proportional to the micropattern width. That is, the amount of the cells migrating across a unit area through a unit physical spatial cue in a unit time decreased as the micropattern width increased. Noticeably, micropatterns with a width of 3 μm showed the highest random motility coefficient although the micropatterns did not have the longest directional persistence time. The reason for this was that the random motility coefficient was also related to the cell migration speed that significantly increased as the micropattern width decreased. All cellular migratory characteristics (*i.e.*, cell migration speed, directional persistence time, and random motility coefficient) measured on the micropatterns with a width of larger than 45.5 ± 3.5 μm were the same as those measured on a flat substrate (control group 2).

These observations about cell migratory characteristics in response to change in the width of micropatterns inform us of the following biological and physiological facts. First of all, the migration speed of the cells guided by micropatterns is faster than that of the cells on a flat substrate (that is, unguided cells). This is because the guided cells keep almost the same morphology defined by the micropatterns and have a relatively weak cell–substrate adhesion force[42] which is known to increase cell migration speed, while the unguided ones frequently change their morphology and have a relatively strong cell–substrate adhesion force which is recognized to impede cell migration speed. Among the cells guided by the micropatterns, the cells migrating on the micropatterns with a narrow width have a longer longitudinal displacement per each migration cycle than the cells on the micropatterns with a wide width, thus cell migration velocity is inversely proportional to the micropattern width. Secondly, there are both ceiling and floor values for micropattern width, related to the amount of physical spatial cues, which influence cell migration speed. For example, the ceiling and floor values of NIH 3T3 fibroblasts are 3 μm (or less) and about 42 to 49 μm, respectively. Thirdly, cellular mechanosensors which receive and respond to external physical spatial cues (micropatterns in this study) are intensively located (or activated) at the circumferential, marginal zone of the cell rather than at the central zone. Fourthly, based on the experimental results about directional persistence time, the width of micropatterns needs to be comparable to cell size before adhesion (*e.g.*,

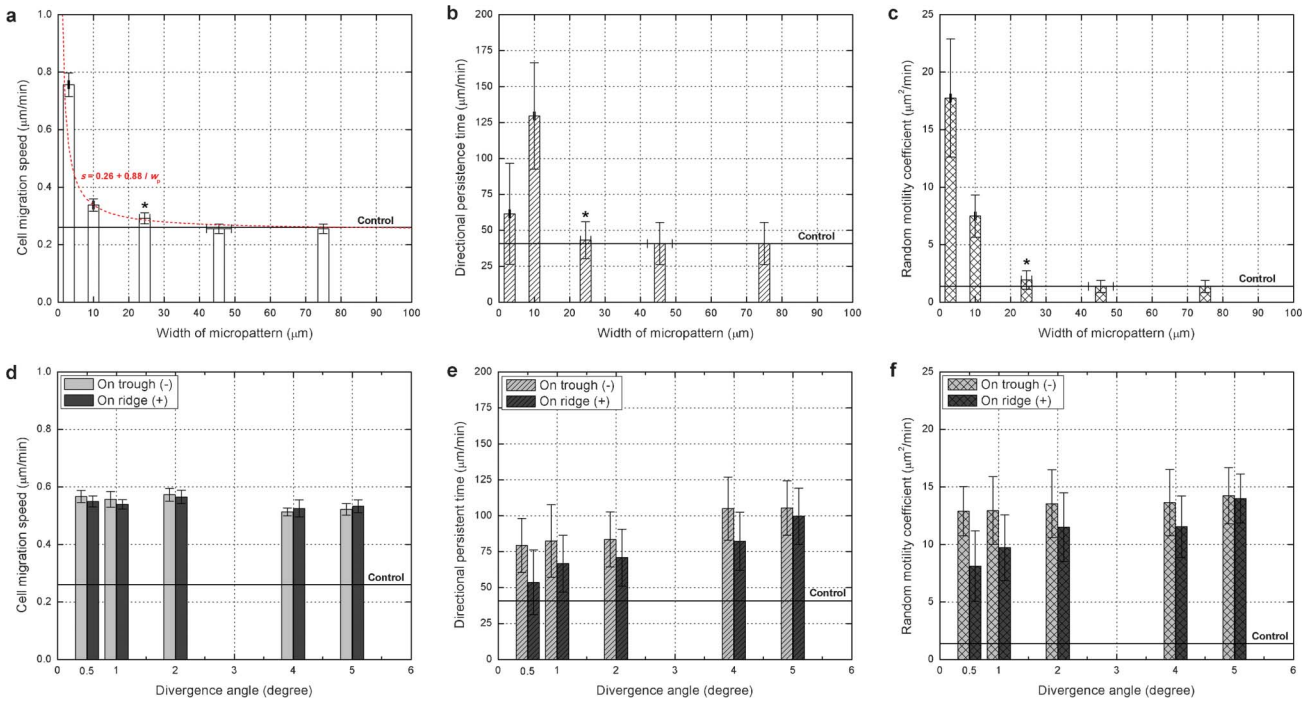

Fig. 6 Quantification of the migratory behavior of NIH 3T3 fibroblasts in response to parallel micropatterns with different micropattern widths (a–c) and diverging micropatterns with different divergence angles (d–f). (a) Cell migration speed, s (μm min^{-1}), as a function of the width of micropatterns, w_c (μm). The measured cell migration speed decreases as the micropattern width increases, expressed as $s = 0.26 + 0.88/w_c$. (b) Directional persistence time as a function of the width of micropatterns. The directional persistence time of NIH 3T3 fibroblasts is maximized when the micropattern width is about 10 μm. (c) Random motility coefficient as a function of the width of micropatterns. The measured random motility coefficient is inversely proportional to the micropattern width. The asterisk symbol denotes the cells migrating on multiple, parallel micropatterns. (d) Cell migration speed as a function of the divergence angle of diverging micropatterns. This shows cell migration speed is almost insensitive to the divergence angle. (e) Directional persistence time as a function of the divergence angle of diverging micropatterns. The measured directional persistence time is also proportional to the divergence angle. (f) Random motility coefficient as a function of the divergence angle of diverging micropatterns. All results are compared with the migratory characteristics obtained from a control group. Error bars of (a–f) are the standard errors of the means.

about 10 μm for NIH 3T3 fibroblasts) to make the cells keep their migration direction for a relatively long time. Last but not least, together with all the above (Fig. 6a–c), micropatterns with a narrower width are of assistance to achieve faster cell migration speed and higher random motility coefficients although the micropatterns have a shorter directional persistence time. Once again, all cellular migratory characteristics except cell migration direction can be successfully controlled through a delicate adjustment of the amount of physical spatial cues (that is, micropattern width in this study).

3.4.2. Dependence of cell migratory characteristics on divergence angle. We also investigated the effect of the divergence angle of micropatterns on cell migratory characteristics using our assay. The cell migration speed was quantified as a function of divergence angle (Fig. 6d). Although micropatterns with divergence (*i.e.*, diverging micropatterns) prominently enhanced cell migration speed compared to a flat substrate, the cell migration speed measured on micropatterns having different divergence angles was identical, showing its insensitivity to the divergence angle. Moreover, the cells on the troughs of diverging micropatterns moved slightly (but not nontrivially) more than those on the ridges, like cell migration on parallel micropatterns (see Table S2 (ESI†)) because the troughs had more stability for cell location than the ridges. Then, the dependence of directional persistence time on the divergence angle of micropatterns was characterized (Fig. 6e). The increase in the divergence angle contributed to increase the directional persistence time; the troughs offered a longer directional persistence time to the cells than the ridges. The former was because the cells on micropatterns with a large divergence angle had relatively high morphological polarity, compared to those on micropatterns with a small one. Again, the blunter leading and sharper trailing edges of adherent cells on micropatterns with a large divergence angle made the cells maintain their migration direction for a longer time. The reason for the latter was that the troughs having two upward sidewalls prevented the cells from crossing the micropatterns (from troughs to ridges) more than the ridges did. Next, the random motility coefficient of NIH 3T3 fibroblasts migrating on diverging micropatterns was studied as a function of divergence angle (Fig. 6f). The random motility coefficient was calculated to be proportional to the divergence angle; the cells migrating on the troughs had a higher random motility coefficient than those migrating on the ridges. This suggested that the level of morphological polarity, determined by the divergence angle, had correlation with random motility coefficient.

Together with all cellular migratory characteristics in response to changes in the width and divergence angle of micropatterns (Fig. 6), we conclude as follows. The amount of physical spatial

cues (*e.g.*, micropattern width in this study) determines the quantitative aspect of all cellular migratory characteristics, while the gradient of physical spatial cues (*e.g.*, divergence angle in this study) decides the directional aspect of them. Therefore, when adherent cells are guided by micropatterns, the cell migration speed is controlled not by divergence angle but by micropattern width, whereas the cell migration direction is adjusted not by micropattern width but by divergence angle. Another finding which claims our attention is that morphological polarization in adherent cells is sufficient to determine the migration direction of the cells whether the morphological polarization is biological (*i.e.*, induced by the gradient of biochemical cues for *in vivo* cell migration) or artificial (*i.e.*, induced by the gradient of physical spatial cues for the passive control of cell locomotion using the Rome platform). Next, these results point out how to design lab-on-a-chip devices that control cell locomotion in a passive way. In detail, when adherent cells are guided using parallel micropatterns, a decrease in the micropattern width enhances both cell migration speed and the random motility coefficient but reduces directional persistence time. When adherent cells migrate on diverging micropatterns, an increase in the divergence angle makes it possible to control cell migration in a specified direction for a relatively long time but has an acceptable loss in maintaining cell migration direction.

4. Conclusions

A new biological assay engraved with micropatterns with different widths of 3 to 75 μm and different divergence angles of 0.5 to 5.0°, nicknamed the "Rome platform," has been developed to passively direct the locomotion of adherent cells. As a preliminary study for developing smart wound dressings, this assay was used to quantitatively characterize the effect of the geometry of micropatterns on the locational and migratory behaviors of adherent cells. In particular, the width and divergence angle of micropatterns were considered as independent variables that represent the amount and gradient of physical spatial cues (*i.e.*, micropatterns) respectively, thus separately exploring their effect on cell locomotion. NIH 3T3 fibroblasts were seeded on the Rome platform that was microfabricated using a biocompatible, UV-curable polymer (ORMOCOMP). The location of the cells migrating on the Rome platform was tracked at every half hour for 48 h using time-lapse microscopy. After measuring the migration path of the cells isolated from each other, the cell migration path was analyzed with a persistent random walk model to quantify all cellular migratory characteristics such as cell migration speed, directional persistence time, and random motility coefficient.

The locational behavior of the cells was successfully controlled by adjusting the micropatterns' geometry, especially micropattern width, informing us that the locational behavior of adherent cells is affected by the amount of physical spatial cues and not by the gradient of them. Noticeably, more cells were located on the troughs than on the ridges because the troughs were like cavities that hindered cell migration from troughs to ridges and enhanced it in the reverse direction. The migratory behavior (*e.g.*, direction and rate of cell migration) was also controllable by deliberately changing the geometry of micropatterns. Cell migration direction was manipulated by creating the gradient of physical spatial cues (that is, divergence angle of micropatterns). In contrast, cell migration speed was controlled by modulating the amount of them (namely, width of micropatterns).

Finally, all the experimental results have verified that the locational and migratory behavior of adherent cell can be controlled by changing the geometry of micropatterns. These findings are expected to give useful propositions for the design of lab-on-a-chip devices that control the locomotion of adherent cells in a passive way. The extrapolation of our results to other adherent cells might help us to better understanding of the migratory nature of adherent cells in response to nano- and microscale physical spatial cues, thus leading to a development of new therapeutic strategies for pathophysiological consequences related to cell migration. Ongoing works are focusing on the synthesis of biodegradable, UV-curable materials for the Rome platform to shed light on the development of smart wound dressings and are planning to investigate molecular biomechanics associated with cell migration with aid of molecular dynamics models.[51,52]

Acknowledgements

Financial support by National Science Foundation through a CAREER award to M.R.K.M. (CBET 0955291) is gratefully acknowledged.

References

1 D. A. Lauffenburger and A. F. Horwitz, *Cell*, 1996, **84**, 359–369.
2 A. J. Ridley, M. A. Schwartz, K. Burridge, R. A. Firtel, M. H. Ginsberg, G. Borisy, J. T. Parsons and A. R. Horwitz, *Science*, 2003, **302**, 1704–1709.
3 V. Jones, K. Harding, J. Stechmiller and G. Schultz, in *Wound Care Essentials: Practice Principles*, ed. S. Baranoski and E. A. Ayello, Lippincott Williams & Wilkins, New York, 2008, pp. 64–76.
4 G. C. Gurtner, S. Werner, Y. Barrandon and M. T. Longaker, *Nature*, 2008, **453**, 314–321.
5 P. Martin and S. M. Parkhurst, *Development*, 2004, **131**, 3021–3034.
6 I. C. Schneider and J. M. Haugh, *Cell Cycle*, 2006, **5**, 1130–1134.
7 S. E. Henrickson, T. R. Mempel, I. B. Mazo, B. Liu, M. N. Artyomov, H. Zheng, A. Peixoto, M. P. Flynn, B. Senman, T. Junt, H. C. Wong, A. K. Chakraborty and U. H. von Andrian, *Nat. Immunol.*, 2008, **9**, 282–291.
8 J. Jacobelli, F. C. Bennett, P. Pandurangi, A. J. Tooley and M. F. Krummel, *J. Immunol.*, 2009, **182**, 2041–2050.
9 A. J. Tooley, J. Gilden, J. Jacobelli, P. Beemiller, W. S. Trimble, M. Kinoshita and M. F. Krummel, *Nat. Cell Biol.*, 2009, **11**, 17–26.
10 D. Hanahan and R. A. Weinberg, *Cell*, 2000, **100**, 57–70.
11 M. Schafer and S. Werner, *Nat. Rev. Mol. Cell Biol.*, 2008, **9**, 628–638.
12 E. S. Witze, E. S. Litman, G. M. Argast, R. T. Moon and N. G. Ahn, *Science*, 2008, **320**, 365–369.
13 R. G. Harrison, *J. Exp. Zool.*, 1914, **17**, 521–544.
14 J. Y. Lim and H. J. Donahue, *Tissue Eng.*, 2007, **13**, 1879–1891.
15 M. N. Yousaf, B. T. Houseman and M. Mrksich, *Proc. Natl. Acad. Sci. U. S. A.*, 2001, **98**, 5992–5996.
16 A. Tourovskaia, T. Barber, B. T. Wickes, D. Hirdes, B. Grin, D. G. Castner, K. E. Healy and A. Folch, *Langmuir*, 2003, **19**, 4754–4764.
17 S. P. Massia and J. A. Hubbell, *J. Cell Biol.*, 1991, **114**, 1089–1100.
18 K. Y. Lee, E. Alsberg, S. Hsiong, W. Comisar, J. Linderman, R. Ziff and D. Mooney, *Nano Lett.*, 2004, **4**, 1501–1506.
19 S. Takeuchi, *Dev. Biol.*, 1976, **51**, 49–62.
20 A. M. Green, J. A. Jansen, J. P. van der Waerden and A. F. von Recum, *J. Biomed. Mater. Res.*, 1994, **28**, 647–653.
21 H. J. Fitton, B. A. Dalton, G. Beumer, G. Johnson, H. J. Griesser and J. G. Steele, *J. Biomed. Mater. Res.*, 1998, **42**, 245–257.
22 M. J. Dalby, D. Giannaras, M. O. Riehle, N. Gadegaard, S. Affrossman and A. S. Curtis, *Biomaterials*, 2004, **25**, 77–83.

23 K. Kolind, A. Dolatshahi-Pirouz, J. Lovmand, F. S. Pedersen, M. Foss and F. Besenbacher, *Biomaterials*, 2010, **31**, 9182–9191.
24 Y. A. Rovensky and V. I. Samoilov, *J. Cell Sci.*, 1994, **107**, 1255–1263.
25 C. Oakley and D. M. Brunette, *Biochem. Cell Biol.*, 1995, **73**, 473–489.
26 A. Curtis and C. Wilkinson, *Biomaterials*, 1997, **18**, 1573–1583.
27 X. F. Walboomers, H. J. Croes, L. A. Ginsel and J. A. Jansen, *Biomaterials*, 1998, **19**, 1861–1868.
28 D. M. Brunette and B. Chehroudi, *J. Biomech. Eng.*, 1999, **121**, 49–57.
29 X. F. Walboomers, W. Monaghan, A. S. Curtis and J. A. Jansen, *J. Biomed. Mater. Res.*, 1999, **46**, 212–220.
30 F. Johansson, P. Carlberg, N. Danielsen, L. Montelius and M. Kanje, *Biomaterials*, 2006, **27**, 1251–1258.
31 H. Jeon, H. Hidai, D. J. Hwang, K. E. Healy and C. P. Grigoropoulos, *Biomaterials*, 2010, **31**, 4286–4295.
32 C. D. Nobes and A. Hall, *J. Cell Biol.*, 1999, **144**, 1235–1244.
33 S. Etienne-Manneville and A. Hall, *Cell*, 2001, **106**, 489–498.
34 A. Kodama, I. Karakesisoglou, E. Wong, A. Vaezi and E. Fuchs, *Cell*, 2003, **115**, 343–354.
35 N. L. Jeon, H. Baskaran, S. K. W. Dertinger, G. M. Whitesides, L. Van de Water and M. Toner, *Nat. Biotechnol.*, 2002, **20**, 826–830.
36 F. Lin, C. Nguyan, S. Wang, W. Saadi, S. Gross and N. L. Jeon, *Ann. Biomed. Eng.*, 2005, **33**, 475–482.
37 J. P. Diao, L. Young, S. Kim, E. A. Fogarty, S. M. Heilman, P. Zhou, M. L. Shuler, M. Wu and M. P. DeLisa, *Lab Chip*, 2006, **6**, 381–388.
38 C. W. Frevert, G. Boggy, T. M. Keenan and A. Folch, *Lab Chip*, 2006, **6**, 849–856.
39 S. Koyama, D. Amarie, H. Soini, M. Novotny and S. C. Jacobson, *Anal. Chem.*, 2006, **78**, 3354–3359.
40 N. Blow, *Nat. Methods*, 2007, **4**, 589–594.
41 R. B. Dickinson and R. T. Tranquillo, *AIChE J.*, 1993, **39**, 1995–2010.
42 P. A. DiMilla, J. A. Stone, J. A. Quinn, S. M. Albelda and D. A. Lauffenburger, *J. Cell Biol.*, 1993, **122**, 729–737.
43 J. Tan and W. M. Saltzman, *Biomaterials*, 2002, **23**, 3215–3225.
44 D. I. Shreiber, V. H. Barocas and R. T. Tranquillo, *Biophys. J.*, 2003, **84**, 4102–4114.
45 C. L. Stokes, D. A. Lauffenburger and S. K. Williams, *J. Cell Sci.*, 1991, **99**, 419–430.
46 A. Ovsianikov, S. Schlie, A. Ngezahayo, A. Haverich and B. N. Chichkov, *J. Tissue Eng. Regener. Med.*, 2007, **1**, 443–449.
47 E. Cukierman, R. Pankov, D. R. Stevens and K. M. Yamada, *Science*, 2001, **294**, 1708–1712.
48 S.-H. Yoon, J. Chang, L. Lin and M. R. K. Mofrad, *Lab Chip*, 2011, **11**, 3555–3562.
49 B. Alberts, A. Johnson, J. Lewis, M. Raff, K. Roberts and P. Walter, *Garland Science*, New York, 2002.
50 S.-H. Yoon and Y.-H. Cho, *J. Microelectromech. Syst.*, 2006, **15**, 967–975.
51 S. E. Lee, S. Chunsrivirot, R. D. Kamm and M. R. K. Mofrad, *Biophys. J.*, 2008, **95**, 2027–2036.
52 J. Golji and M. R. K. Mofrad, *Biophys. J.*, 2010, **99**, 1073–1081.